
Article:
Malone, L.A., Qian, P., Mayneord, G.E. et al. (7 more authors) (2019) Cryo-EM structure of the spinach cytochrome b6 f complex at 3.6 Å resolution. Nature. ISSN 0028-0836

https://doi.org/10.1038/s41586-019-1746-6

Cryo-EM structure of the spinach cytochrome b_6f complex at 3.6 Å resolution

Lorna A. Malone[1], Pu Qian[1], Guy E. Mayneord[1], Andrew Hitchcock[1], David A. Farmer[1], Rebecca F. Thompson[2], David J.K. Swainsbury[1], Neil A. Ranson[2], C. Neil Hunter[1,3*], Matthew P. Johnson[1,3*]

[1]Department of Molecular Biology and Biotechnology, Firth Court, University of Sheffield, Western Bank, S10 2TN.
[2]Astbury Centre for Structural Molecular Biology, School of Molecular & Cellular Biology, Faculty of Biological Sciences, University of Leeds, LS2 9JT

[3]These authors jointly supervised this work

*e-mail: c.n.hunter@sheffield.ac.uk; matt.johnson@sheffield.ac.uk.

The cytochrome b_6f (cytb_6f) complex plays a central role in oxygenic photosynthesis, linking electron transfer between photosystems I and II and conserving solar energy as a transmembrane proton gradient for ATP synthesis[1-3]. Electron transfer within cytb_6f occurs via the Q-cycle, which catalyses the oxidation of plastoquinol (PQH_2) and the reduction of both plastocyanin (PC) and plastoquinone (PQ) at two separate sites via electron bifurcation[2]. In higher-plants cytb_6f also acts as a redox-sensing hub, pivotal to the regulation of light harvesting and cyclic electron transfer that protect against metabolic and environmental stresses[3]. Here we present a 3.6 Å resolution cryo-electron microscopy (cryo-EM) structure of the dimeric cytb_6f complex from spinach, which reveals the structural basis for operation of the Q-cycle and its redox sensing function. The complex contains up to three natively bound PQ molecules. The first, PQ1, is bound to one cytb_6f monomer at the PQ oxidation site (Q_p) adjacent to haem b_p and chlorophyll *a*. Two conformations of the chlorophyll *a* phytyl tail were resolved, one that prevents access to the Q_p site and another that permits it, supporting a gating function for the chlorophyll *a* involved in redox sensing. PQ2 straddles the intermonomer cavity, partially obstructing the PQ reduction site (Q_n) on the PQ1 side and committing the electron transfer network to turnover at the occupied Q_n site in the neighbouring monomer. A conformational switch involving the haem c_n propionate promotes two-electron, two-proton reduction at the Q_n site and avoids formation of the reactive intermediate semiquinone. The location of a tentatively assigned third PQ molecule is consistent with a transition between the Q_p and Q_n sites in opposite monomers during the Q-cycle. The spinach cytb_6f structure therefore provides new insights into how the complex fulfils its catalytic and regulatory roles in photosynthesis.

Photosynthesis sustains life on Earth by converting light into chemical energy in the form of ATP and NADPH, producing oxygen as a by-product. Two light-powered electron transfer reactions at photosystems I and II (PSI and PSII) are linked via the cytb_6f complex to form the so-called 'Z-scheme' of photosynthetic linear electron transfer (LET)[1]. Cytb_6f catalyses the rate-limiting step in the LET chain, coupling the oxidation of PQH_2 and reduction of PC and PQ to the generation of a transmembrane proton gradient (Δp), used by ATP synthase to make ATP[2,3]. The cytb_6f complex is analogous to the cytochrome bc_1 (cytbc_1) complex found in mitochondria[4] and anoxygenic photosynthetic bacteria[5] and both operate via the modified Q-

cycle[2,6]. Both cytb_6f and cytbc_1 are dimeric and have similarly arranged electron transfer co-factors, comprising a 2Fe-2S cluster, two *b*-type haems and a *c*-type haem. However, crystallographic structures of cyanobacterial and algal cytb_6f complexes revealed additional co-factors not found in cytbc_1 complexes, including a chlorophyll *a*, a 9-*cis* β-carotene and an extra *c*-type high-spin haem[7-9]. The Q-cycle involves bifurcated transfer of the two electrons, derived from oxidising a lipophilic PQH_2 molecule at the Q_p binding site, into the high (2Fe-2S, cyt*f*) and low (cytb_p, b_n and c_n) redox potential pathways, while the two protons enter the thylakoid lumen[2,6]. The high potential pathway delivers an electron to a membrane-extrinsic soluble acceptor protein, PC, destined for PSI, while the low potential pathway delivers its electron to a PQ molecule bound at the Q_n site near the stromal side of the membrane. Oxidation of a second PQH_2 at the Q_p site leads to the two-electron reduction of a Q_n site bound PQ, which together with two proton transfers from the stroma, regenerates PQH_2[2,6]. The Q-cycle thereby doubles the number of protons transferred to the lumen per PQH_2 oxidised. Yet, full understanding of the Q-cycle mechanism is hindered by a lack of information on the binding of the substrate PQ/ PQH_2 molecules within the complex.

In addition to its role in LET, cytb_6f also plays a key role as a redox sensing hub involved in the regulation of light harvesting and cyclic electron transfer (CET), which optimise photosynthesis in fluctuating light environments[10,11]. Cytb_6f communicates the redox status of the PQ pool to the loosely associated light harvesting complex II (LHCII) kinase, STN7[12-14]. Phosphorylation of LHCII results in a decrease in thylakoid membrane stacking, promoting the exchange of LHCII between PSII and PSI to balance their relative excitation rates[15] and regulate CET[16]. CET involves the reinjection of electrons from Ferredoxin (Fd) into the PQ pool, generating Δp, for photoprotective downregulation of PSI and PSII or to augment ATP synthesis, without net formation of NADPH[11]. The cytb_6f complex has been proposed to fulfil the role of the Fd-PQ oxidoreductase (FQR) during CET, with the stromal-facing haem c_n suggested to channel electrons from Fd $NADP^+$ reductase (FNR) bound Fd to the Q_n site PQ[17]. How cytb_6f performs these central redox sensing regulatory roles remains unclear. Nonetheless, genetic manipulation of photosynthetic regulation is now recognised as being key to increasing crop yields to feed a global population projected to approach 10 billion by 2050[18]. Indeed, overproduction of the Rieske iron-sulphur protein (ISP) of cytb_6f in *Arabidopsis thaliana* led to a 51% increase in yield[19]. Further progress in understanding the regulatory roles of cytb_6f and potentially manipulating them for crop improvement requires the structure of the higher plant complex. Here, using a gentle purification procedure to obtain a highly active dimeric complex (Extended Data Fig. 1) and single-particle cryo-EM we resolve the cytb_6f complex from *Spinacia oleracea* (spinach) at 3.6 Å resolution (Extended Data Fig. 2 and Extended Data Table 1).

The colour-coded map (Fig. 1a, b, c) shows the architecture of this dimeric complex surrounded by a disordered density comprising detergent and lipid molecules. The overall organisation of this higher plant cytb_6f complex is similar to crystallographic structures of algal and cyanobacterial complexes from *Chlamydomonas reinhardtii*[7] (PDB ID: 1Q90), *Mastigocladus laminosus*[8] (PDB ID: 1VF5) and *Nostoc* sp. PCC

7120[9] (PDB ID: 2ZT9) (Extended Data Table 2). Each monomeric unit of the cytb_6f complex comprises four large polypeptide subunits that contain redox cofactors (cyt *f*, cyt b_6, ISP, subIV), and four small subunits (PetG, L, M, N). Extended Data Fig. 3 shows the density and structural model for each subunit. The extrinsic domains of cyt *f* and the ISP on the lumenal face of the complex flank the membrane-integral cyt b_6 subunits (Fig. 1a, b). The organisation of the transmembrane integral subunits can be seen on the stromal side of the complex (Fig. 1c) with 13 transmembrane helices (TMH) visible within each monomer (Fig 1d, e, f). Peripheral to the core of cyt b_6 (four TMH) and subIV (three TMH) on the long axis of the complex is the single kinked TMH of the ISP that crosses over to provide the soluble ISP domain of the neighbouring monomer. The single TMH belonging to cyt *f* is sandwiched by the TMH of the four minor subunits PetG, L, M and N, which form a 'picket-fence' at the edge of the complex.

Fig. 2a, b show the organisation of the prosthetic groups and lipids, with four *c*-type haems (*f* and c_n, dark blue), four *b*-type haems (b_p and b_n, red), two 2Fe-2S clusters (orange-yellow), two 9-*cis* β-carotenes (orange), two chlorophyll (Chl) *a* molecules (green), three PQ molecules (yellow) and twelve bound lipids (two monogalactosyldiacylglycerol, four phosphatidylglycerol, three sulfoquinovosyldiacylglycerol and three phosphatidylcholine, all shown in white). Extended Data Fig. 4 shows the density map and structural model for each prosthetic group. Fig 2c shows all the bound electron transfer cofactor edge-to-edge distances within the cytb_6f complex. Electron transfer from the 2Fe-2S cluster is thought to involve movement of the lumenal ISP domain, pivoting between closer association with the Q_p site and the haem *f*[20]. By comparison with the chicken cytbc_1 complex where the two conformations of the ISP were resolved, in the spinach cytb_6f structure the ISP and bound 2Fe-2S cluster appear to be in the distal position with respect to haem *f*, as in the existing algal and cyanobacterial cytb_6f structures (Extended Data Table 2). PQ locations are generally inferred from crystallographic structures containing tightly bound quinone analogue inhibitors[21-23]; here, the spinach cryo-EM structure was obtained with native PQ molecules (Fig. 2d), clearly defined by their respective densities (Extended Data Fig. 4) with their distances from the closest co-factors shown in Fig 2e-g. One PQ molecule (PQ1) is found adjacent to the haem b_p and Chl on one side of the dimer (Fig. 2e), and a second (PQ2) binds adjacent to the haem c_n - haem b_n pair on the opposite monomer to PQ1 (Fig. 2f). A third and less clearly defined PQ (PQ3) lies between the haem c_n of one monomer and the haem b_n of the other (Fig. 2g). The density map in this region can also be assigned to a phospholipid and Extended Data Figure 5 shows the two possible fits, to a quinone or lipid

The 1,4-benzoquinone ring of PQ1 is 16.2 Å from haem b_p and 26.4 Å from the 2Fe-2S cluster (Fig. 2e) and distal to the Q_p quinone oxidising site, defined in the *M. laminosus* cytb_6f structure[23] (PDB ID: 4H13) by the inhibitor tridecylstigmatellin (TDS) (Fig. 3a,b). The Q_p site is located within a pocket formed by hydrophobic residues from subIV (Val84, Leu88, Val98, Met101) and cyt b_6 (Phe81, Val126, Ala129, Val133, Val151, Val154) (Fig. 3c). Since bifurcated electron transfer to the 2Fe-2S cluster and haem b_p involves two deprotonation events mediated by the His128 (ISP) and Glu78 (subIV) residues[2,3], which are buried inside

the Q_p pocket (Fig. 3a,b), it seems unlikely that PQ1 is oxidised in its resolved position, since its -OH group is some ~26 Å from His128, a ligand to the 2Fe-2S cluster (Fig. 3b), and is more likely a snapshot of its approach. It is interesting in this regard that our spinach cytb_6f structure resolves two conformations of the Chl phytyl tail, one of which permits access to Q_p site, while the second restricts it (Fig. 3c,d). There is only one position of the phytyl tail for the Chl on the opposing monomer. In this way the bound Chl adjacent to PQ1 may fulfil a gating function at the Q_p pocket, either controlling access of PQH_2 and/or increasing the retention time of the reactive semiplastoquinone (SPQ) intermediate species formed following electron transfer to the 2Fe-2S cluster. Indeed, spin-coupling between the SPQ to the 2Fe-2S cluster has been detected during enzymatic turnover of cytb_6f but is absent in cytbc_1 complexes which lack the Chl molecule[24]. SPQ in the FeS-bound state does not react with oxygen, which provides a potential mechanism to control release of superoxide from the Q_p site[24] and to regulate the activity of the LHCII kinase STN7[25], which is proposed to bind to cytb_6f between the F and H TMH of subIV[26]. Another role for Chl in regulating the activity of STN7, could involve PQH_2 displacing the Chl phytyl tail upon binding to the Q_p site and this motion could induce a conformational change in STN7 leading to its activation[27].

PQ2 binds towards the stromal face of the complex 4.4 Å from the haem c_n / b_n pair at the Q_n reducing site (Fig. 2f). The b_n and c_n haems on each monomer are separated by 4.9 Å, with the b_n haem coordinated by His202/100 (cyt b_6) and the vinyl side-chain of haem c_n covalently linked to Cys35 (cyt b_6) (Fig. 2f). The dimerisation interface of the cytb_6f complex creates a cavity, proposed to promote transfer of quinones between the Q_p and Q_n sites on neighbouring monomers[8] (Fig. 4a, b). It is significant in this regard that all three resolved PQ molecules inhabit this cavity and that PQ2 assumes a position 'diagonally' opposite to PQ1 (Fig. 4c) on the other monomer, as depicted by Nawrocki et al[28]. Notably, PQ2 adopts a bowed conformation that straddles the intermonomer cavity and the distal PQ2 tail appears to partially obstruct the Q_n site in the neighbouring monomer (Fig. 4d, e). This arrangement may have functional significance in preventing the simultaneous binding of PQ molecules at both Q_n sites, avoiding competition for electrons and favouring faster turnover of the Q-cycle. Rapid provision of two electrons for PQ2 bound at a particular Q_n site could be facilitated by the 15.3 Å electron-tunnelling distance between b_p haems (Fig. 2b), which allows rapid inter-monomer electron transfer via the 'bus-bar' model from the neighbouring low potential chain[29,30]. Alternatively, the second electron could be provided to the haem c_n directly via a FNR-Fd complex bound at the stromal surface via CET[17,28]. The haem c_n propionates on the two halves of the cytb_6f dimer adopt different conformations (Fig. 4f, g); in the PQ-vacant site on the opposing monomer the haem c_n propionate is more closely associated with Arg207 (Fig. 4f), whereas in the PQ-occupied site the haem c_n propionate is twisted towards the 1,4-benzoquinone ring of PQ2 (Fig. 4g). The altered ligation of haem c_n upon PQ binding is consistent with the downshift of its redox potential[31], which would strongly favour PQ reduction. We note that the reduction/oxidation of haem c_n is accompanied by the binding/release of one proton[31] so only one proton is required from the stromal side via the Arg207 and Asp20 residues (Fig 4f, g) and PQ2 reduction could proceed rapidly, avoiding SPQ formation. It is also possible to position an

oppositely oriented PQ within the density map, albeit with a less satisfactory fit (Extended Data Fig. 5). A third PQ molecule (PQ3) (Fig. 2g) has been assigned to the density between the Q_p and Q_n binding sites (see Extended Data Fig. 6 for an alternative assignment as phosphatidylcholine) with the 1,4 benzoquinone ring near to the channel that links the two sides of the intermonomer cavity and the isoprenyl tail at the mouth of the Q_p site. This third PQ may therefore capture a snapshot of the molecule transitioning between the Q_p and Q_n sites in opposite monomers.

The cryo-EM structure of spinach cytb_6f reveals the positions of the natively bound PQ complement and provides new details regarding the conformational switches involved in PQ binding to the Q_n site, Chl gating of the Q_p site and PQ exchange between the sites during Q-cycle operation.

REFERENCES

1. Hill, R. & Bendall, F. Function of the two cytochrome components in chloroplasts: a working hypothesis. *Nature* **186**, 136-137 (1960).
2. Cramer, W.A., Hasan, S.S., & Yamashita, E. The Q cycle of cytochrome *bc* complexes: A structure perspective. *Biochim. Biophys. Acta* **1807,** 788–802 (2011).
3. Tikhonov, A.N. The cytochrome b_6f complex at the crossroad of photosynthetic electron transport pathways. *Plant Physiol. Biochem.* **81**, 163e183 (2014).
4. Xia, D., Yu, C.A., Kim, H., Xia, J.Z., Kachurin, A.M., Zhang, L., Yu, L. & Deisenhofer, J. Crystal structure of the cytochrome bc_1 complex from bovine heart mitochondria. *Science* **277**, 60–66 (1997).
5. Esser, L., Elberry, M., Zhou, F., Yu, C.A., Yu, L., & Xia, D. Inhibitor-complexed structures of the cytochrome bc_1 from the photosynthetic bacterium *Rhodobacter sphaeroides. J. Biol. Chem*. **283**, 2846–2857 (2007).
6. Cape, J.L., Bowman, M.K. & Kramer, D.M. Understanding the cytochrome *bc* complexes by what they don't do. The Q-cycle at 30. *Trends Plant Sci.* **11**, 46-52 (2006).
7. Stroebel, D., Choquet, Y., Popot, J.-L., & Picot, D. An atypical haem in the cytochrome b(6)f complex. *Nature* **426**, 413–418 (2003).
8. Kurisu, G., Zhang, H., Smith, J. L., & Cramer, W. A. Structure of the cytochrome b_6f complex of oxygenic photosynthesis: Tuning the cavity, *Science* **302**, 1009-1014 (2003).
9. Baniulis, D., Yamashita, E., Whitelegge, J. P., Zatsman, A. I., Hendrich, M. P., Hasan, S. S., Ryan, C. M., and Cramer, W. A. (2009) Structure-function, stability, and chemical modification of the cyanobacterial cytochrome b_6f complex from Nostoc sp. PCC 7120. *J. Biol. Chem*. 284, 9861–9869
10. Bellafiore, S., Barneche, F., Peltier, G. & Rochaix, J.D. State transitions and light adaptation require chloroplast thylakoid protein kinase STN7. *Nature* 433, 892–895 (2005)

11. Yamori, W. & Shikanai, T. Physiological functions of cyclic electron transport around photosystem I in sustaining photosynthesis and plant growth. *Annu. Rev. Plant Biol.* **67**, 81-106 (2016).
12. Horton, P. & Black, M. T. Activation of adenosine 5'-triphosphate induced quenching of chlorophyll fluorescence by reduced plastoquinone. The basis of state I-state II transitions in chloroplasts. FEBS Lett. 119, 141-144 (1980).
13. Vener, A.V., van Kan, P.J., Rich, P.R., Ohad, I., Andersson, B. Plastoquinol at the quinol oxidation site of reduced cytochrome *bf* mediates signal transduction between light and protein phosphorylation: thylakoid protein kinase deactivation by a single-turnover flash. *Proc. Nat. Acad. Sci. USA* **94**, 1585–1590 (1997).
14. Gal, A., Hauska, G., Herrmann, R. & Ohad, I. Interaction between light harvesting chlorophyll-a/b protein (LHCII) kinase and cytochrome b_6/f complex. *J. Biol. Chem.* 265, 19742-19749 (1990).
15. Allen, J. F., Bennett, J., Steinback, K. E. & Arntzen, C. J. Chloroplast protein phosphorylation couples plastoquinone redox state to distribution of excitation energy between photosystems. *Nature* **291,** 25-29 (1981).
16. Wood, W.H.J., MacGregor-Chatwin, C., Barnett, S., Mayneord, G., Huang, X., Hobbs, J., Hunter, C.N. & Johnson, M.P. Dynamic thylakoid stacking regulates the balance between linear and cyclic photosynthetic electron transfer. *Nature Plants* **4**, 116–127 (2018).
17. Zhang, H., Whitelegge, J.P. & Cramer, W.A. Ferredoxin:$NADP^+$ Oxidoreductase Is a Subunit of the Chloroplast Cytochrome b_6f Complex. *J. Biol. Chem.* 276, 38159-38165 (2001).
18. Zhu, X.G., Long, S.P. & Ort, D.R. Improving photosynthetic efficiency for greater yield. *Ann. Rev. Plant Biol.* **61**, 235–261 (2010).
19. Simkin, A.J., McAusland, L., Lawson, T. & Raines, C.A. Overexpression of the Rieske FeS protein increases electron transport rates and biomass yield. *Plant Physiol*. **175**, 134–145 (2017).
20. Zhang, Z., Huang, L., Schulmeister, V., Chi, Y-I., Kim, K.K., Hung, L-W., Crofts., A.R., Berry, E. A. & Kim, S-H. Electron transfer by domain movement in cytochrome bc_1. *Nature,* 392, 677-684 (1998).
21. Yan, J., Kurisu, G. & Cramer, W. A. Structure of the cytochrome b_6f complex: binding site and intra-protein transfer of the quinone analogue inhibitor 2,5- dibromo-3-methyl-6-isopropyl-p-benzoquinone. *Proc. Natl Acad. Sci. USA.* 103, 67–74 (2006).
22. Yamashita, E., Zhang, H. & Cramer, W. A. Structure of the cytochrome b_6f complex: quinone analogue inhibitors as ligands of heme c_n. *J. Mol. Biol.* **370**, 39–52 (2007).
23. Hasan, S.S., Yamashita, E., Baniulis, D. & Cramer, W.A. Quinone-dependent proton transfer pathways in the photosynthetic cytochrome b_6f complex. *Proc. Nat. Acad. Sci. USA* 110, 4297-4302 (2013)
24. Sarewicz, M., Bujinowicz, L., Bhaduri, S., Singh, S.K., Cramer, W.A. & Osyckza, A. Metastable radical state, nonreactive with oxygen, is inherent to catalysis by respiratory and photosynthetic cytochromes bc_1/b_6f. *Proc. Nat. Acad. Sci. U. S. A.* 114, 1323-1328 (2017).

25. Singh, S.K. et al. Trans-membrane signalling in photosynthetic state transitions. *J. Biol. Chem*. **291**, 21740-21750 (2016).
26. Zito, F., Vinh, J., Popot, J. L., and Finazzi, G. Chimeric fusions of subunit IV and PetL in the b_6f complex of *Chlamydomonas reinhardtii:* structural implications and consequences on state transitions. *J. Biol. Chem.* **277**, 12446 –12455 (2002).
27. Hasan, S.S, Yamashita, E., & Cramer, W. A. Transmembrane signaling and assembly of the cytochrome b_6f-lipidic charge transfer complex. *Biochim. Biophys. Acta* **1827**, 1295–1308 (2013).
28. Nawrocki, W.J., Bailleul, B., Picot, D., Cardol, P., Rappaport, F. & Wollman, F.A. The mechanism of cyclic electron flow. *Biochim. Biophys. Acta* **1860**, 433-438 (2019).
29. Osyczka, A., Moser, C. C., Daldal, F., & Dutton, P. L. Reversible redox energy coupling in electron transfer chains. *Nature* **427**, 607-612 (2004).
30. Świerczek, M., Cieluch, E., Sarewicz, M., Borek, A., Moser, C. C., Dutton, P. L., & Osyczka, A. An electronic bus bar lies in the core of cytochrome bc_1. *Science* **329**, 451-454 (2010).
31. Alric, J., Pierre, Y., Picot, D., Lavergne, J. & Rappaport, F. Spectral and redox characterization of the heme c_i of the cytochrome b_6f complex. *Proc. Nat. Acad. Sci. USA* **102,** 15860 –15865 (2005).

ACKNOWLEDGMENTS

M.P.J. acknowledges funding from the Leverhulme Trust grant RPG-2016-161. C.N.H., P.Q., A.H., D.J.K.S. and M.P.J. also gratefully acknowledge financial support from the Biotechnology and Biological Sciences Research Council (BBSRC UK), award numbers BB/M000265/1, BB/P002005/1. L.A.M was supported by a White Rose doctoral studentship, G.E.M. was supported by a doctoral studentship from The Grantham Foundation and D.F. was supported by a University of Sheffield doctoral scholarship. CryoEM data was collected at the Astbury Biostructure Laboratory funded by the University of Leeds (ABSL award) and the Wellcome Trust (108466/Z/15/Z). Dr Svet Tzokov, Dr Julien Bergeron, Dr Jason Wilson and Dr Daniel Mann (University of Sheffield) are acknowledged for their helpful advice and assistance with the EM and data processing.

AUTHOR CONTRIBUTIONS

P.Q, C.N.H, N.R and M.P.J supervised the project. L.A.M., G.E.M, P.Q., C.N.H., R.F.T and M.P.J. designed the experiments. L.A.M. and G.E.M. purified the cytochrome b_6f complex, L.A.M., G.E.M., A.H. and D.J.K.S. characterised the cytochrome b_6f complex, L.A.M., P.Q., D.A.F. and R.F.T. collected, processed and/or analysed the cryo-EM data. L.A.M., C.N.H. and M.P.J. wrote the manuscript. All authors proofread and approved the manuscript.

COMPETING INTERESTS

The authors declare no competing interests

FIGURE LEGENDS

Fig. 1 | Cryo-EM structure of the cytb_6f complex from spinach. a-c, Views of the colour-coded cytb_6f density map showing cytochrome b_6 (cyt b_6, green), cytochrome *f* (cyt *f*, magenta), ISP (yellow), subunit IV (subIV, cyan), PetG (grey), PetM (pale purple), PetN (pale orange), PetL (pink). Detergent and other disordered molecules are shown in semi-transparent light grey. **a,** View in plane of the membrane. The grey stripe indicates the likely position of the thylakoid membrane bilayer. **b,** View perpendicular to the membrane plane from the lumenal (p) side. **c,** View perpendicular to the membrane plane from the stromal (n) side. **d-f,** Modelled subunits of cytb_6f shown in a cartoon representation and coloured as in **a**-**c.**

Fig. 2 | The global arrangement of prosthetic groups, lipids and plastoquinone molecules in the spinach cytb_6f complex. a-b, The arrangement of molecules in the cytb_6f complex viewed in the membrane plane **(a)** and perpendicular to the membrane plane from the stromal side **(b). c-d,** Cofactors and edge-to-edge distances (Å) in the dimeric cytb_6f complex. **e**, The location of the 1,4-benzoquinone ring of PQ1 adjacent to haem b_p, the 2Fe-2S centre and two conformations of the Chl molecule, represented in two shades of green. **f**, Close-up of the 1,4-benzoquinone ring of PQ2 and nearby haem c_n and haem b_n near the stromal face of the complex. **g**, The 1,4-benzoquinone ring of PQ3, which sits between the haem c_n and haem b_n from the two cytb_6f monomers. The cytb_6f complex is coloured as in Fig 1, and shows *c*-type haems (*f,* c_n; dark blue), *b*-type haems (b_p, b_n; red), 9-*cis* β-carotene (car; orange), chlorophyll *a* (Chl; green), 2Fe-2S (FeS; orange/yellow), lipids (white) and plastoquinones (PQ1-3; yellow).

Fig. 3 | Conformational alterations in the Chl phytyl chain at the PQH_2-oxidising Q_p site. a, Disposition of the PQ1 in relation to the haem b_p, Chl and 2Fe-2S cofactors. The catalytically essential residue E78 is shown, as are coordinating residues of the 2Fe-2S cofactor. TDS is a quinone analogue, superimposed according to its position determined in the cyanobacterial complex (PDB ID: 4H13)[23], and used here to indicate the likely destination for PQ1 in the Q_p pocket. **b**, The same cofactors and residues as in **a**, but now in relation to a surface view of cyt b_6 (green) and SubIV (cyan). **c**, The Q_p pocket is highlighted with a purple dashed line in relation to the Chl and PQ1 molecules; the hydrophobic residues of subIV (cyan) and cyt b_6 that line the pocket are shown as sticks and coloured cyan and green respectively. **d**, The two conformations of the Chl tail (represented in dark green and light green) gate (dashed arrow) the entrance to the Q_p pocket.

Fig. 4 | The intermonomer cavity of the spinach cytb_6f complex. a-b, Surface representations of the complex, with subunits coloured as in Fig. 1, and cofactors and lipids as in Fig. 2. These two views of the complex are related by a 45° rotation about an axis perpendicular to the membrane, to show two views of

the cavity and the locations of PQ molecules. **c**, PQ1-3 are shown in relation to the b_n, c_n and b_p haems in the core of the complex, viewed in the membrane plane. **d**, The complex viewed from the stromal side of the membrane; peripheral helices of cyt b_6 and subIV are shown in cartoon representation for clarity, to show PQ2 straddling the intermonomer cavity and sitting between the two c_n haems. **e**, Close-up of the cavity in panel (**d**). **f-g**, The head and tail regions of PQ2 in relation to the c_n haems on both sides of the cavity, highlighting the different dispositions of the haem c_n propionates, and the Arg207 and Asp20 sidechains.

METHODS

Complex purification

Dimeric cyt b_6f was isolated from dark-adapted market spinach *(Spinacia oleracea)* in a procedure adapted from Dietrich and Kuhlbrandt[32].

Briefly, spinach leaves were homogenised in Buffer 1 (50 mM Tris-HCl pH 7.5, 200 mM sucrose, 100 mM NaCl). Homogenate was then filtered and centrifuged for 15 min at 4540 RCF, 4°C. Following centrifugation, the supernatant containing cell debris was discarded and the pellet resuspended in Buffer 2 (150 mM NaCl, 10 mM Tricine-NaOH pH 8) before centrifugation again for 15 min (4540 RCF, 4°C). The resultant pellet was resuspended in Buffer 3 (2 M NaBr, 10 mM Tricine-NaOH pH 8, 300 mM sucrose) and incubated on ice for 15 min before diluting 2-fold with ice cold milliQ H_2O and centrifuging (15 min, 4540 RCF, 4°C). The resultant pellet was resuspended in Buffer 3 and incubated on ice for 15 min before diluting 2-fold with ice cold milliQ H_2O and centrifuging again (15 min, 4540 RCF, 4°C). The pellet was resuspended in Buffer 2 and centrifuged for 15 min, 4540 RCF, 4°C. The final pellet was resuspended in a small volume of Buffer 4 (40 mM Tricine pH 8.0, 10 mM $MgCl_2$, 10 mM KCl). The resultant thylakoid suspension was adjusted to 10 mg ml^{-1} Chl (Chl concentrations determined as described by Porra et al.[33]).

For selective solubilisation of cyt b_6f , the thylakoid suspension (10 mg ml^{-1} Chl) was diluted with Membrane Extraction Buffer (40 mM Tricine pH 8.0, 10 mM $MgCl_2$, 10 mM KCl, 1.25% (w/v) Hecameg) to a final concentration of 2 mg ml^{-1} Chl, 1% (w/v) Hecameg. The resultant solution was mixed thoroughly then incubated for 2 mins at room temperature before dilution to 0.75% (w/v) Hecameg with Buffer 4. Unsolubilised material was removed by ultracentrifugation at 244,000 RCF at 4°C for 30 min in a Beckman Ti50.2 rotor.

The solubilisation supernatant was concentrated using a Centriprep 100K centrifugal filter (Merck Millipore Ltd.) before loading onto a 10-40% (w/v) continuous sucrose gradient containing 40 mM Tricine pH 8, 10 mM $MgCl_2$, 10 mM KCl, 0.8% (w/v) Hecameg, 0.1 mg ml^{-1} egg yolk L-α-phosphatidylcholine (Sigma). This was ultracentrifuged at 174,587 RCF at 4°C for 16 h in a Beckman SW32 rotor.

A brown-ish band containing cyt b_6f was harvested from a region of the gradient corresponding to ~16% sucrose. This band was concentrated and loaded onto a ceramic hydroxyapatite column (CHT) (Type I, Bio-Rad) pre-equilibrated in 20 mM Hecameg, 0.1 mg ml^{-1} Phosphatidylcholine, 20 mM Tricine pH 8. The column was washed with 5 column volumes of CHT Wash Buffer (20 mM Hecameg, 0.1 mg ml^{-1} Phosphatidylcholine, 100 mM ammonium phosphate pH 8) before bound material was eluted with CHT Elution Buffer (20 mM Hecameg, 0.1 mg ml^{-1} Phosphatidylcholine, 400 mM ammonium phosphate pH 8).

Detergent exchange and gel filtration

Concentrated CHT eluate was loaded onto a 10-35% (w/v) continuous sucrose gradient containing 50 mM HEPES pH 8, 20 mM NaCl, 0.3 mM tPCCαM and ultracentrifuged at 175,117 RCF at 4°C for 16 h in a Beckman SW41 rotor.

A single brown band containing cyt b_6f was harvested from a region of the gradient corresponding to ~22% sucrose. This band was concentrated and loaded onto HiLoad 16/600 Superdex 200 pg gel filtration column (GE Healthcare) connected to an ÄKTA prime plus purification system (GE Healthcare). The column was run at a rate of 0.2 ml min^{-1} with 145 ml with Gel Filtration Buffer (50 mM HEPES pH 8, 20 mM NaCl, 0.3 mM tPCCαM). Eluted fractions comprising dimeric cyt b_6f were pooled and concentrated.

SDS-PAGE and BN-PAGE analysis

Samples collected from each purification step were analysed by SDS-PAGE and BN-PAGE. For SDS-PAGE, precast NuPAGE 12% Bis-Tris gels (Invitrogen) were run for 60 min at 180 V before staining with Coomassie Blue. For BN-PAGE, precast NativePAGE 3-12% Bis-Tris gels (Invitrogen) were run for 120 min at 160 V before staining with Coomassie Blue. Gels were imaged using an Amersham 600 imager (GE Healthcare).

Quantification of purified dimeric cytochrome b_6f using redox difference spectra

Absorbance spectra were recorded at room temperature on a Cary60 spectrophotometer (Agilent). For redox difference spectra cytochromes were first fully oxidised with a few grains of potassium ferricyanide followed by reduction with a few grains of sodium ascorbate (cyt *f*) then sodium dithionite (cyts *f* and b_6). At each stage the sample was mixed thoroughly and incubated for ~1 min before recording spectra. Redox difference spectra (ascorbate-reduced minus ferricyanide-oxidised and dithionite-reduced minus ascorbate-reduced) were calculated and used to determine the concentrations of cyt *f* and the two *b*-type cyts using extinction coefficients of 25 mM cm^{-1} (*f*) and 21 mM cm^{-1} (b_6)[34].

Reduction of decylplastoquinone

Approximately 0.1 mg decylplastoquinone (Merck, UK) was dissolved in 100 µl ethanol, mixed with a few grains of sodium dithionite dissolved in 100 µl milliQ H_2O and vortexed until the solution became colourless. Decylplastoquinol was extracted by mixing with 0.5 ml hexane, vortexing and centrifuging at 16,000 RCF for 2 mins. The hexane layer was carefully removed ensuring none of the aqueous phase was collected. Hexane extraction was repeated on the aqueous phase twice more, then the hexane solutions were pooled and dried in a rotary evaporator at 30 °C for 1 hour prior to re-dissolving in ~100 µl DMSO. Decylplastoquinol concentration was determined by dilution of 10 µl of the DMSO solution into 795 µl ethanol, recording the absorbance spectrum between 250 and 350 nm and using an extinction coefficient of 3540 M^{-1} cm^{-1} at 290 nm[35].

Activity assays

Reduction of PC by cyt b_6f was monitored by stopped-flow absorbance spectroscopy using an Olis RSM 1000 rapid-scanning spectrophotometer equipped with a USA-SF stopped flow cell at 20 °C. Solution A (231.25 nM cyt b_6f and 62.5 µM PC in 50 mM HEPES pH 8, 20 mM NaCl, 0.3 mM tPCCαM) and solution B (1.25 mM decylplastoquinol in the same buffer) were prepared and the reaction was initiated by mixing the solutions in a 4:1 volumetric ratio (final concentrations: 185 nM cyt b_6f, 50 µM PC, 250 µM decylplastoquinol). PC reduction was monitored by recording absorbance spectra between 420-750 nm at a rate of 62 scans sec^{-1} and plotting the change in absorbance at 597 nm[36]. In a control reaction cyt b_6f was omitted to record the uncatalysed reduction of PC by decylplastoquinol. Fitting of the initial reaction rates was performed in Origin. All measurements were carried out in triplicate.

Purification of plastocyanin

Plastocyanin was purified in its oxidised form from market spinach. Briefly, spinach leaves were homogensied in buffer containing 50 mM sodium phosphate pH 7.4, 5 mM $MgCl_2$, 300 mM sucrose. Homogenate was then filtered and centrifuged for 15 min at 4000 RCF. Following centrifugation, the supernatant containing cell debris was discarded and the pellet resuspended in buffer containing 10 mM Tricine pH 7.4, 5 mM $MgCl_2$. The solution was incubated on ice for 1 min before diluting 2-fold with buffer containing 10 mM Tricine pH 7.4, 5 mM $MgCl_2$, 400 mM sucrose and centrifuging for 15 mins at 4000 RCF. Following centrifugation, the pellet was resuspended to a chlorophyll concentration of 2 mg ml^{-1} in buffer containing 10 mM HEPES pH 7.6, 5 mM NaCl, 5 mM EDTA, and sonicated for 10 min, at 30 sec intervals. The solution was centrifuged at 200,000 RCF for 1 h to pellet any large unbroken material. The supernatant was applied to 4 x 5 ml GE Healthcare Hi-TRAP Q FF anion exchange columns chained together, equilibrated in

HEPES pH 8, 5 mM NaCl. A gradient of 0.005-1 M NaCl was used for elution, with PC eluting at around 200 mM. PC-containing fractions were identified by the blue colour upon addition of potassium ferricyanide. These fractions were pooled, concentrated in a Vivaspin 3 kDa molecular-weight cut-off spin concentrator and loaded onto a Superdex™ 200 16/600 FPLC column, equilibrated with 20 mM HEPES pH 8, 20 mM NaCl. The resulting PC fractions were pooled, concentrated, and frozen at -80°C until use.

CryoEM specimen preparation and data acquisition

3 µl of purified cyt b_6f (~17µM) was applied to freshly glow discharged holey carbon grids (Quantifoil R1.2/1.3, 400 mesh Cu). The grids were blotted for 2 sec at 8^{o}C then plunge frozen into liquid ethane using a Leica EM GP at 90% relative humidity. Data acquisition was carried out on a Titan Krios microscope operated at 300 kV (Thermo Fisher) equipped with an energy filtered (slit width 20 eV) K2 summit direct electron detector. A total of 6,035 movies were collected in counting mode at a nominal magnification of 130,000 X (pixel size of 1.065 Å) and a dose of 4.6 e^{-} Å^{-2} s^{-1} (see Extended Data Table 1). An exposure time of 12 sec was used and the resulting movies were dose-fractionated into 48 fractions. A defocus range of -1.5 to -2.5 µm was used.

Image processing and 3D reconstruction

Beam-induced motion correction and dose-fractionation were carried out using MotionCor2. Contrast transfer function (CTF) parameters of the dose-weighted motion corrected images were then estimated using GCTF[37]. All subsequent processing steps were performed using RELION 2.1[38] or 3.0[39] unless otherwise stated.

In total, 422,660 particles were manually picked from 6,035 micrographs. These particles were extracted using a box size of 220 x 220 pixels and subjected to reference-free 2D classification. A typical micrograph showing picked particles is shown in Extended Data Fig. 2a,b. Particles that categorised into poorly defined classes were rejected, while the remaining 292,242 (69.2%) particles were used for further processing. A subset of 30,000 particles was used to generate a *de novo* initial model using the '3D initial model' subroutine. The initial model low pass filtered to 20 Å was used as a reference map for subsequent 3D classification into 10 3D classes. One stable 3D class at a resolution of 5.38 Å was selected for high resolution 3D auto-refinement; this class accounted for a subset of 108,560 particles (25.6%). This subset of refined particles was then re-extracted and re-centred before another round of 3D auto refinement was carried out. The resultant 4.85 Å density map was corrected for the modulation transfer function (MTF) of the Gatan K2 summit camera then further sharpened using the post-processing procedure to 4.02 Å. Per-particle CTF-refinement was carried out and a soft mask was created which included the detergent shell.

The final global resolution estimate of 3.58 Å was based on the gold-standard Fourier shell correlation (FSC) cut off of 0.143.

Local resolution was determined using one of two unfiltered half-maps as an input, a calibrated pixel size of 1.065 and a B-factor of -103. The output local resolution map is shown in Extended Data Fig 2d,e.

Model building

Initially, a homology-based approach was performed using the crystallographic structure of *Nostoc* sp. PCC 7120 cyt b_6f (PDB: 4OGQ)[40] as a template. Sequence alignments of the 8 polypeptide subunits of cyt b_6f were carried out using Clustal Omega (Extended Data Fig. 7 and 8). The model was rigid-body docked into the density using the 'fit in map' tool in Chimera[41]. This was then followed by manual adjustment and real-space refinement using COOT[42]. Sequence assignment and fitting was guided by bulky residues such as Arg, Trp, Tyr and Phe. After fitting of the polypeptide chains and cofactors in one half of the dimeric complex, the other half of the complex was then independently fitted into the C1 density map. Once both halves of the complex were fitted, cofactors, lipids and plastoquinone-9 molecules were fitted into regions of unassigned density. The final model underwent global refinement and minimisation using the real space refinement tool in PHENIX[43]. The final refinement statistics are summarised in Extended Data Table 1.

Pigment analysis by reversed-phase HPLC

Pigments were extracted from purified cytb_6f with 7:2 acetone/methanol (v/v) and clarified extracts were separated by reversed-phase HPLC at a flow rate of 1 ml min^{-1} at 40°C using a Supelco Discovery® HS C18 column (5 µm particle size, 120 Å pore size, 25 cm × 4.6 mm) on an Agilent 1200 HPLC system. The column was equilibrated in acetonitrile: water: trimethylamine (9:1:0.01 v/v/v) and pigments were eluted by applying a linear gradient of 0-100% ethyl acetate over 15 min followed by isocratic elution with 100% ethyl acetate for a further 5 min. Elution of carotenoid and chlorophyll species was monitored by absorbance at 400, 450, 490 and 665 nm. Chlorophyll *a* was identified by its absorption spectra and known retention time[44]. The major carotenoid species was confirmed as 9-*cis* beta-carotene using a standard obtained from Sigma-Aldrich (Product number: 52824).

DATA AVAILABILITY STATEMENT

All relevant data are available from the authors and/or are included with the manuscript or Supplementary Information. Atomic coordinates and the cryo-EM density map have been deposited in the Protein Data

Bank (PDB) under accession number 6RQF and the Electron Microscopy Data Bank (EMDB) under accession number EMD-4981.

METHODS REFERENCES

32. Dietrich, J. & Kuhlbrandt, W. Purification and two-dimensional crystallization of highly active cytochrome b6f complex from spinach. FEBS Lett **463,** 97–102 (1999).
33. Porra, RJ, Thompson, WA and Kriedemann, PE. Determination of accurate extinction coefficients and simultaneous equations for assaying chlorophylls *a* and *b* extracted with four different solvents: verification of the concentration of chlorophyll standards by atomic absorption spectroscopy. *Biochim Biophys Acta* **975**, 384– 394. (1989)
34. Cramer, W.A. & Whitmarsh, J. Photosynthetic cytochromes. *Ann. Rev. Plant Physiol*. **28**, 133-172 (1977)
35. Dawson, R. M. C., Elliot, D. C., Elliot, W. H., and Jones, K. M. Data for Biochemical Research, p. 132, Clarendon Press, Oxford (1986)
36. Tan, S. & Ho, K.K. Purification of an acidic plastocyanin from *MicroBiomis aeruginosa. Biochim. Biophys. Acta* **973**, 111-117 (1989)
37. Zhang, K. Gctf: Real-time CTF determination and correction. *J. Struct. Biol.* **193**, 1–12 (2016).
38. Fernandez-Leiro, R., & Scheres, S. H. W. A pipeline approach to single-particle processing in RELION. *Acta Crystallogr. D Struc. Biol.* **73**, 496–502 (2017).
39. Zivanov, J., Nakane, T., Forsberg, B. O., Kimanius, D., Hagen, W. J., Lindahl, E., & Scheres, S. H. New tools for automated high-resolution cryo-EM structure determination in RELION-3. *ELife* ***7,*** 1–38 (2018).
40. Hasan, S.S. & Cramer, W.A. Internal Lipid Architecture of the Hetero-Oligomeric Cytochrome b_6f Complex. *Structure* **22**, 1008-1015 (2014).
41. Pettersen, E. F. et al. UCSF Chimera—a visualization system for exploratory research and analysis. *J. Comput. Chem.* **25**, 1605–1612 (2004).
42. Adams, P. D. *et al.* PHENIX: a comprehensive Python-based system for macromolecular structure solution. *Acta Crystallogr. D Biol. Crystallogr*. **66,** 213–221 (2010).
43. Emsley, P. & Cowtan, K. Coot: model-building tools for molecular graphics. *Acta Crystallogr*. D **60**, 2126–2132 (2004).
44. Proctor, M.P., Chidgey, J.W., Shukla, M.K., Jackson, P.J., Sobotka, R., Hunter, C.N. & Hitchcock, A. Plant and algal chlorophyll synthases function in Synechocystis and interact with the YidC/Alb3 membrane insertase. FEBS Lett. **592**, 3062-3073 (2018).

Extended Data Table 1. Cryo-EM data collection, refinement and validation statistics. *Peter B Rosenthal and Richard Henderson (2003) Optimal determination of particle orientation, absolute hand and contrast loss in single particle electron cryomicroscopy. J. Mol. Biol., 333(4):721-745.

Extended Data Table 2. A comparison of edge-to-edge cofactor distances (Å) in each half of the b_6f dimer from different species (6RQF, 1Q90, 2E74, 4OGQ) and the bc_1 dimer from *G. gallus* with the Rieske ISP in its distal (1BCC) and proximal (3BCC) positions. * Inhibitors are indicated by the abbreviations TDS (tridecylstigmatellin), STG (stigmatellin), AMY (antimycin).

Extended Data Figure 1. Purification of cytochrome b_6f from spinach. **a,** Absorption spectrum of ascorbate-reduced purified b_6f complex. The peak at 421nm corresponds to the Soret band of bound pigments (chlorophyll *a* and haems). The peaks at 554 and 668 nm correspond to *c*-type haem of cytochrome *f* and chlorophyll *a* respectively. The inset panel shows a redox difference spectra of ascorbate-reduced minus ferricyanide-oxidised b_6f (dashed line) and dithionite-reduced minus ascorbate-reduced (dotted line) cytb_6f. Redox difference spectra show cytochrome *f* absorption peaks at 523 and 554 nm as well as absorption peaks at 534 and 563nm corresponding to the *b*-type cytochromes of cytochrome b_6. The calculated ratio of cytochrome b_6 to cytochrome *f* was ~2 using extinction coefficients of 25 mM cm^{-1} (*f*) and 21 mM cm^{-1} (b_6) (Cramer and Whitmarsh, 1977). The spectra exhibit the absorption properties characteristic of intact cytochrome b_6f. Spectra were recorded at room temperature. **b,** SDS-PAGE analysis of purified cytochrome b_6f indicates the sample is highly pure with the four large subunits of the complex (cyt *f,* cyt b_6, the Rieske ISP, subunit IV) running at ~31 kDa, ~24 kDa, ~20 kDa and ~17 kDa respectively and the 4 small subunits (PetG, L, M,and N) running at around 4 kDa (not shown). **c-d,** Negative stain and BN-PAGE analysis of purified cytochrome b_6f demonstrates the sample is dimeric and highly homogenous, with a single band corresponding to dimeric cytochrome b_6f shown in lane 1. Lane 2 is a sample which has been deliberately monomerised following incubation with 1% Triton-X-100 for 1 hour. For gel source data see Supplementary Information Figure 1. **e,** The catalytic rate of plastocyanin reduction by the purified dimeric cytb_6f complex as determined by stopped-flow absorbance spectroscopy. A rate of 200 $e^- s^{-1}$ was determined by taking the initial linear region from the enzyme-catalysed reaction (solid line) and deducting the background rate measured in the absence of enzyme (long-dashed line). Plastocyanin reduction was not observed in the absence of decylplastoquinol (short dashed line). Reactions were initiated upon addition of decylplastoquinol to the solution containing plastocyanin and b_6f whist monitoring the loss of absorbance at 597nm. Final concentrations were 50 µM plastocyanin, 185 nm b_6f and 250 µM decylplastoquinol. All experiments were performed in triplicate and controls were performed in the absence of b_6f or decylplastoquinol.

Extended Data Figure 2. **Cryo-EM micrographs of the spinach cytochrome b_6f complex and calculation of the cryo-EM map global and local resolution. a**, Cytochrome b_6f particles covered by a thin layer of vitreous ice on a supported carbon film. **b**, Examples of dimeric cytochrome b_6f particles are circled in green. 6,035 cryo-EM movies were recorded, from which 422,660 particles were picked manually for reference-free 2D classification. 108,560 particles were used for calculation of the final density map. **c**, Gold standard refinement was used for estimation of the final map resolution (solid black line). The global

resolution of 3.58 Å was calculated using a Fourier shell correlation (FSC) cut-off at 0.143. A model-to-map FSC curve (solid grey line) was also calculated. **d-e,** A C1 density map of the cytochrome b_6f complex both with **(d)** and without **(e)** the detergent shell. The map is coloured according to local resolution estimated by RELION and viewed from within the plane of the membrane. The colour key on the right shows the local structural resolution in Angstroms (Å).

Extended Data Figure 3. Cryo-EM densities and structural models of polypeptides in the cytochrome b_6f complex. Polypeptides are coloured as in Fig. 1. The contour levels of the density maps were adjusted to 0.0144

Extended Data Figure 4. Cryo-EM densities and structural models of prosthetic groups, lipids and plastoquinone molecules in the cytochrome b_6f complex. *c*-type haems (*f, c*$_n$; dark blue), *b*-type haems (b_p, b_n; red), 9-*cis* β-carotene (orange), chlorophyll *a* (major conformation, dark green) (minor conformation, light green), 2Fe-2S (orange/yellow), plastoquinones (yellow), monogalactosyl diacylglycerol (light pink), phosphatidylcholine (light cyan), sulfoquinovosyl diacylglycerol (light green), phosphatidylglycerol (light purple). The contour levels of the density maps were adjusted to 0.0068.

Extended Data Figure 5. **Alternative interpretation of the region assigned as PQ2.** The density map showing two possible alternative conformations for PQ2. **a)** The major conformation of PQ2 and **b)** the alternative conformation of PQ2. Cofactors are coloured as in Extended Data Figure 4 with *b*-type haems (b_p, b_n) coloured red, *c*-type haems (c_n) coloured dark blue, chlorophyll *a* (major conformation) coloured dark green, plastoquinones coloured yellow and the cytochrome b_6 subunit coloured light green. The contour level of the density map was adjusted to 0.0089.

Extended Data Figure 6. **Alternative interpretations of the density map in the region assigned as PQ3.** The density map modelled with **(a)** a plastoquinone molecule and **(b)** a phosphatidylcholine molecule. Upper panels show the protein-free density map and the lower panels include cyt b_6 (green). The 2.9 Å distance indicates a close contact between the PQ3 head group and the conserved Lys208. Cofactors are coloured as in Extended Data Figure 4 with *b*-type haems (b_p, b_n) coloured red, chlorophyll *a* (major conformation) coloured dark green, plastoquinones coloured yellow, phosphatidylcholine coloured light cyan, sulfoquinovosyl diacylglycerol coloured mint green, and the cytochrome b_6 subunit coloured light green. The contour level of the density map was adjusted to 0.0127.

Extended Data Figure 7. **Multiple sequence alignment of cytochrome b_6f subunits cytochrome *f*, cytochrome b_6.** Sequences of cytochrome *f* **(a)**, cytochrome b_6 **(b)** from cyanobacterial (*Mastigocladus laminosus, Nostoc* sp. PCC7120), algal (*Chlamydomonas reinhardtii*) and plant (*Spinacia oleracea*) subunits were aligned in Clustal Omega v 1.2.4. Conserved identities are indicated by asterisks (*), and similarities by double (:), then single dots (.). Polar residues are coloured in green, positively charged residues are

coloured pink, hydrophobic residues are coloured red and negatively charged residues are coloured blue. The sequences omit signal peptides.

Extended Data Figure 8. **Multiple sequence alignment of the Rieske ISP, Subunit IV, PetG, PetL, PetM and PetN.** Sequences of Rieske ISP **(a)**, Subunit IV **(b)**, PetG **(c)**, PetL **(d)**, PetM **(e)** and PetN **(f)** from cyanobacterial (*Mastigocladus laminosus, Nostoc* sp. PCC7120), algal (*Chlamydomonas reinhardtii*) and plant (*Spinacia oleracea*) subunits were aligned in Clustal Omega v 1.2.4. Conserved identities are indicated by asterisks (*), and similarities by double (:), then single dots (.). Polar residues are coloured in green, positively charged residues are coloured pink, hydrophobic residues are coloured red and negatively charged residues are coloured blue. The sequences omit signal peptides.

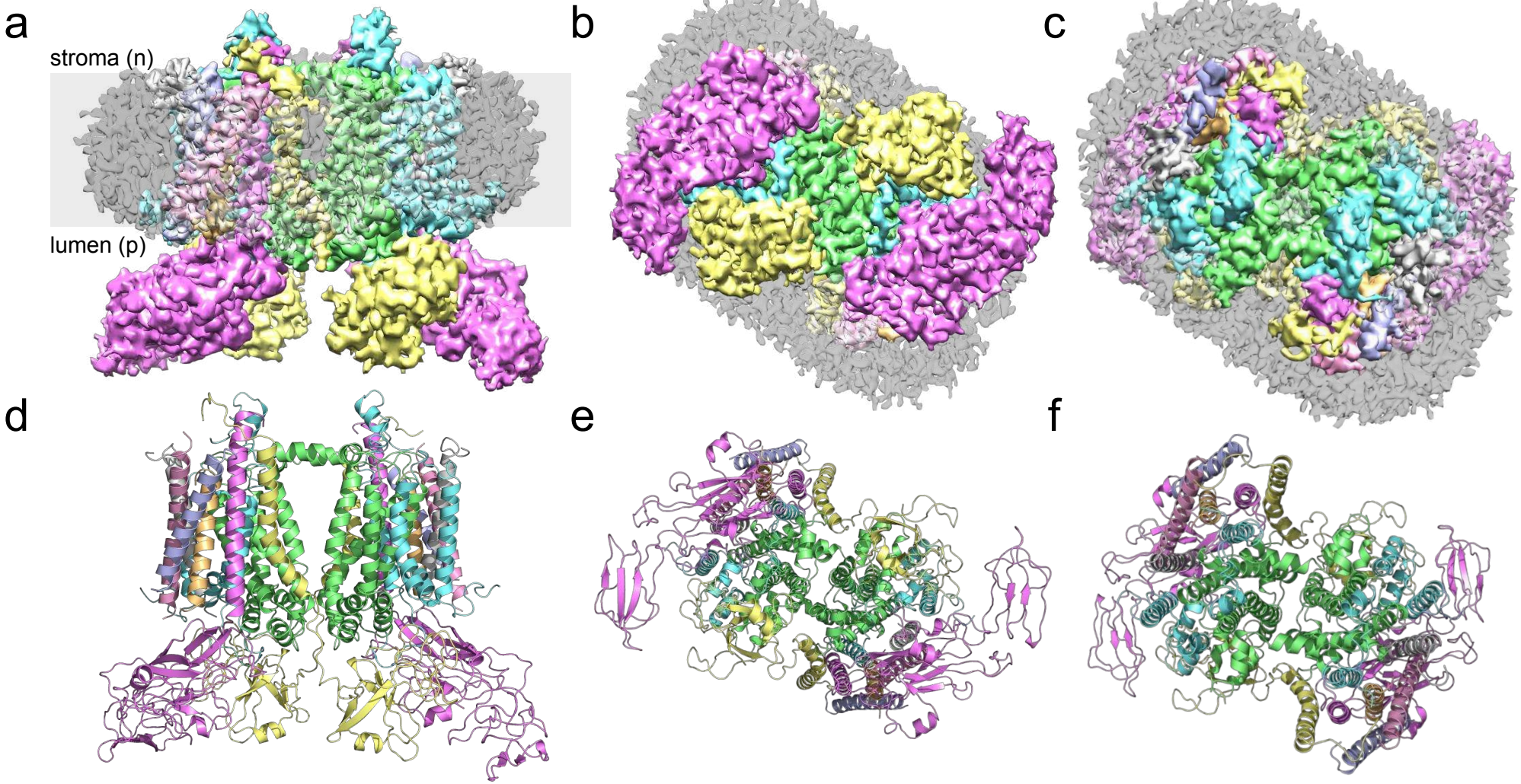
a
stroma (n)
lumen (p)
b
c
d
e
f

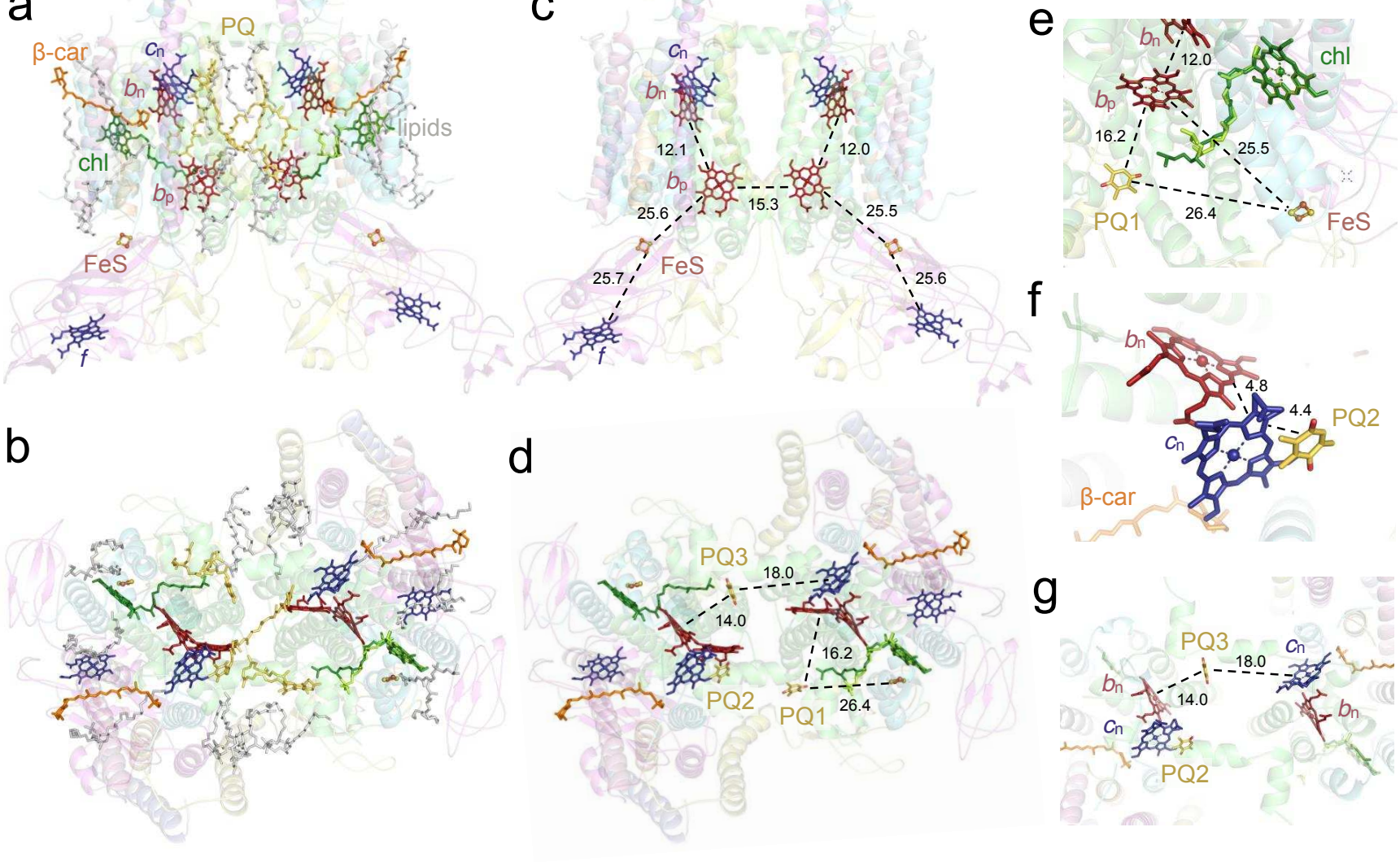
a
PQ
β-car
c_n
b_n
lipids
chl
b_p
FeS
f
c
c_n
b_n
12.1
12.0
b_p
15.3
25.6
25.5
FeS
25.7
25.6
f
e
b_n
12.0
chl
b_p
16.2
25.5
PQ1
26.4
FeS
f
b_n
4.8
4.4
PQ2
c_n
β-car
b
d
PQ3
18.0
14.0
16.2
PQ2
PQ1
26.4
g
PQ3
c_n
18.0
b_n
14.0
c_n
b_n
PQ2

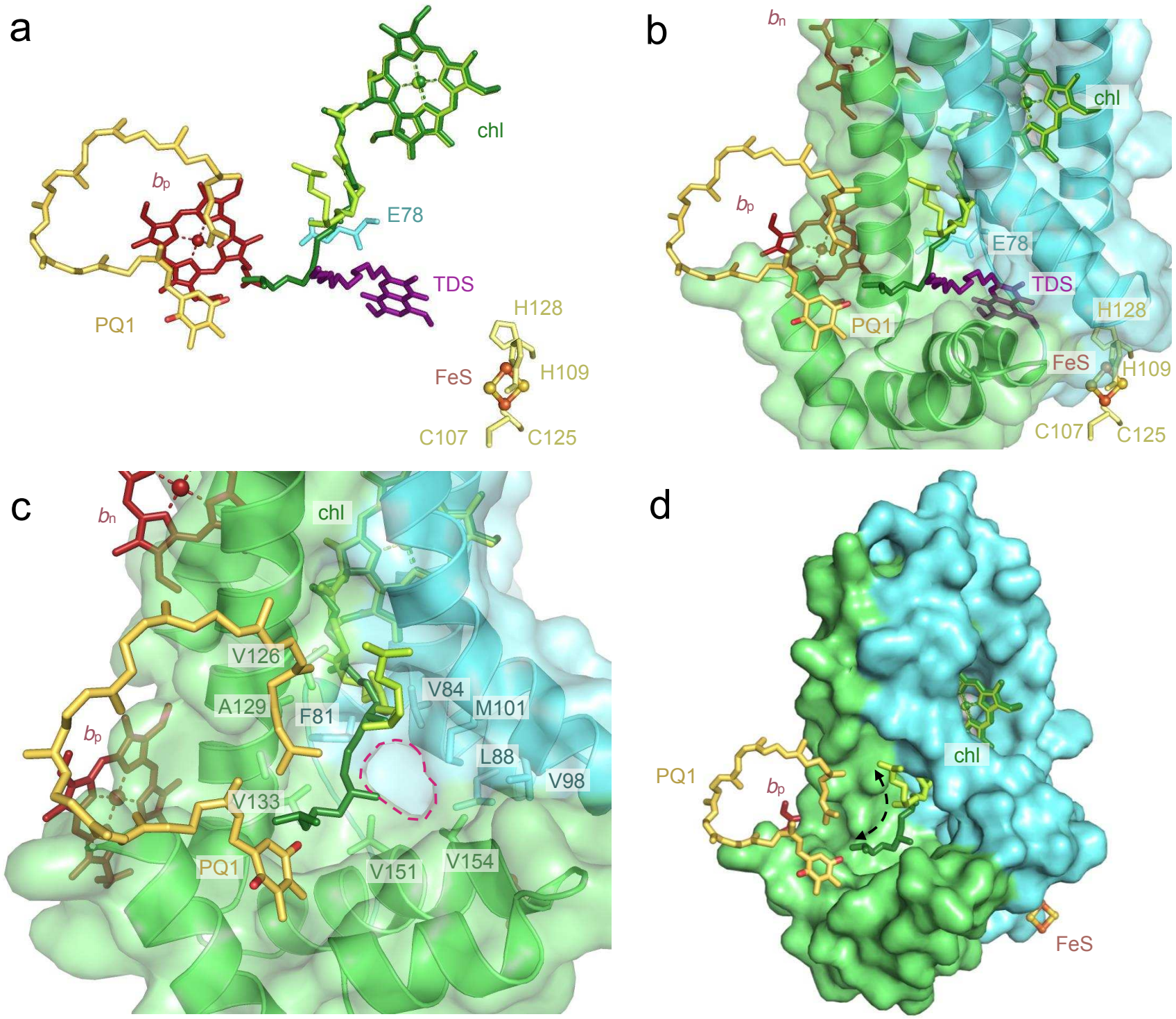
a
chl
b_p
E78
TDS
PQ1
H128
FeS
H109
C107
C125
b
b_n
chl
b_p
E78
TDS
PQ1
H128
FeS
H109
C107
C125
c
b_n
chl
V126
A129
F81
V84
M101
b_p
L88
V98
V133
PQ1
V151
V154
d
PQ1
b_p
chl
FeS

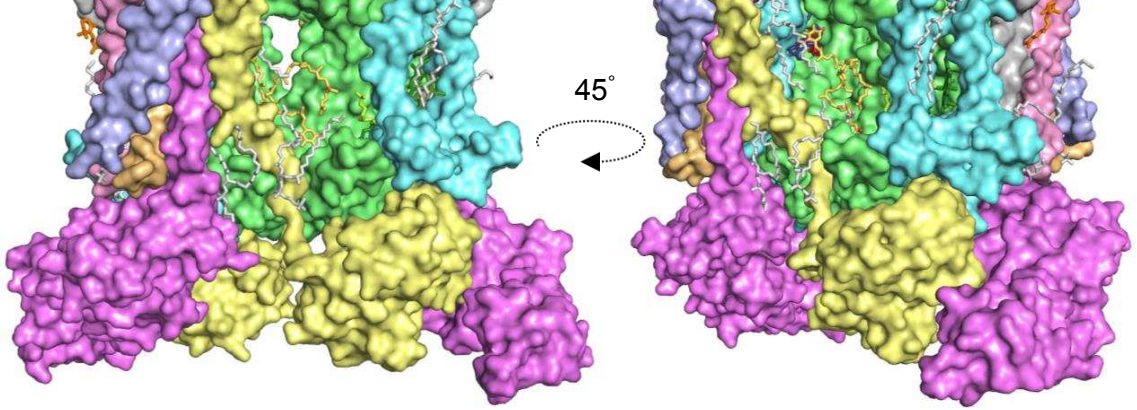
45˚

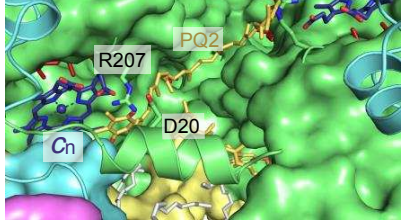
PQ2
R207
D20
cn

f

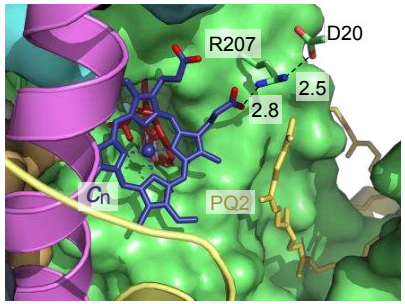
R207
D20
2.5
2.8
cn
PQ2

c

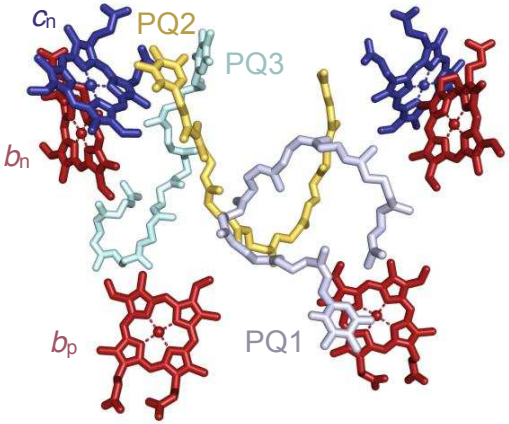
cn
PQ2
PQ3
bn
bp
PQ1

d

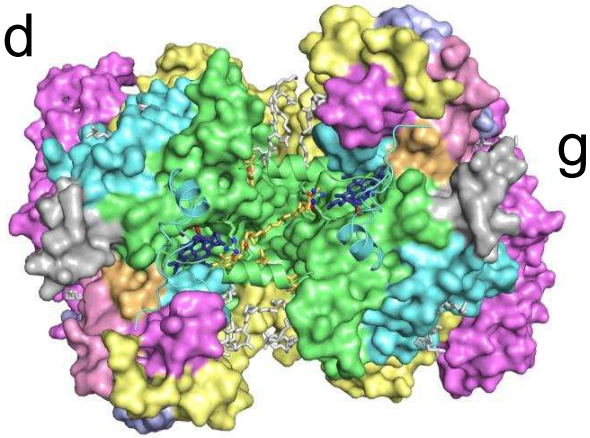

g

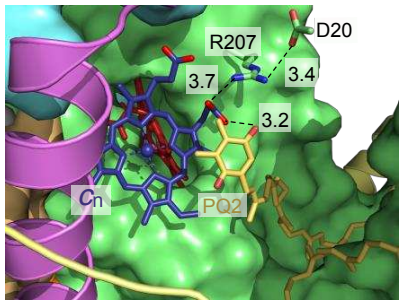
R207
D20
3.7
3.4
3.2
cn
PQ2